

A Pentacyclic Aurora Kinase Inhibitor (AKI-001) with High in Vivo Potency and Oral Bioavailability[∞]

Thomas E. Rawson,[†] Matthias R  th,[‡] Elizabeth Blackwood,[§] Dan Burdick,[†] Laura Corson,[#] Jenna Dotson,[†] Jason Drummond,[†] Carter Fields,[§] Guy J. Georges,[‡] Bernhard Goller,[⊥] Jason Halladay,[†] Thomas Hunsaker,[#] Tracy Kleinheinz,[†] Hans-Willi Krell,^{||} Jun Li,[†] Jun Liang,[†] Anja Limberg,[‡] Angela McNutt,[§] John Moffat,[†] Gail Phillips,[§] Yingqing Ran,[†] Brian Safina,[†] Mark Ultsch,[∇] Leslie Walker,[†] Christian Wiesmann,[∇] Birong Zhang,[†] Aihe Zhou,[†] Bing-Yan Zhu,[†] Petra R  ger,^{||} and Andrea G. Cochran^{*∇}

Departments of Small Molecule Drug Discovery, Cell Cycle and Global Regulators, Translational Oncology, and Protein Engineering, Genentech, Inc., 1 DNA Way, South San Francisco, California 94080, and Departments of Medicinal Chemistry, Cell Biology, and HTS and Biochemistry, Pharma Research, Roche Diagnostics GmbH, D-82372 Penzberg, Germany

Received January 18, 2008

Aurora kinase inhibitors have attracted a great deal of interest as a new class of antimetabolic agents. We report a novel class of Aurora inhibitors based on a pentacyclic scaffold. A prototype pentacyclic inhibitor **32** (AKI-001) derived from two early lead structures improves upon the best properties of each parent and compares favorably to a previously reported Aurora inhibitor, **39** (VX-680). The inhibitor exhibits low nanomolar potency against both Aurora A and Aurora B enzymes, excellent cellular potency (IC₅₀ < 100 nM), and good oral bioavailability. Phenotypic cellular assays show that both Aurora A and Aurora B are inhibited at inhibitor concentrations sufficient to block proliferation. Importantly, the cellular activity translates to potent inhibition of tumor growth in vivo. An oral dose of 5 mg/kg QD is well tolerated and results in near stasis (92% TGI) in an HCT116 mouse xenograft model.

Introduction

Aurora kinases are a family of mitotic serine/threonine kinases conserved from yeast to humans, and they have received significant recent attention as new targets for anticancer therapy.^{1–4} The two major Aurora kinases, Aurora A and Aurora B, have distinct functions in mitosis.^{5–7} Aurora A localizes predominantly to the centrosome, and it is important for proper centrosome maturation and separation. The kinesin HsEg5 (KSP) is also required for centrosome separation,⁸ and Eg5, at least in frog extracts, is a direct substrate of Aurora A.⁹ HsEg5 has itself been the target of anticancer drug discovery efforts.³ Loss or inhibition of either Aurora A¹⁰ or Eg5¹¹ arrests replicating cells in early mitosis with a characteristic monopolar spindle phenotype. Aurora B is required for phosphorylation of histone H3 at serine 10 in early mitosis, prior to chromosome condensation.¹² Aurora B is also a critical component of the spindle assembly checkpoint¹³ and maintains a "wait anaphase" signal until all replicated chromosomes achieve correct biorientation and attachment.¹⁴ Accordingly, loss of Aurora B function can lead to premature anaphase and associated errors in chromosome segregation.^{15,16} Finally, Aurora B is required to complete cytokinesis.¹⁷ Pharmacological inhibition or siRNA knockdown of Aurora B leads to very large multinucleated cells, resulting from repeated rounds of DNA synthesis with no intervening cell division.^{15,16} The third Aurora kinase,

Aurora C, has a kinase domain most similar in sequence to that of Aurora B,¹⁸ and Aurora C appears to have functions that overlap with those of Aurora B.^{19,20} However, the expression pattern of Aurora C is very restricted,¹⁸ and a comprehensive view of its function has yet to emerge.

The initial motivation to direct drug discovery efforts to Aurora kinases arose from early findings that Aurora A in particular is highly expressed in many tumor types and that this overexpression is in some cases driven by amplification of the chromosomal region (20q13) on which the Aurora A gene resides.^{21,22} In some cell lines, overexpression of Aurora A is reported to be transforming.^{22,23} It does not, however, appear that Aurora A can be considered a classic oncogene. There are cell lines that are not transformed by Aurora A,^{22,24} and transgenic mice inducibly overexpressing Aurora A do not develop tumors with high frequency.²⁵ Instead, it appears that elevation of Aurora A may play a supporting role in tumor progression, perhaps in concert with p53 loss-of-function or other mutations, or that a more extended period of overexpression may be required for tumor development.²⁶ Alternatively, a high Aurora A level may be simply a consequence of a high mitotic index in a particular tumor type.³ These questions have yet to be resolved and are under active investigation and debate.

Despite uncertainty surrounding the role of Aurora kinases in tumorigenesis, it is clear that both Aurora A and Aurora B are critical for completion of mitosis and for accurate cell cycle progression. As such, drugs targeting these kinases might be expected to have potent antimetabolic and antitumor activity. The concept of targeting Aurora kinases with small molecule inhibitors has been validated recently in mouse xenograft studies from several groups.^{27–31} Advanced programs exist at many companies,³² and several of these Aurora inhibitors have recently entered the clinic.³ We report here a new Aurora kinase inhibitor

[∞] Coordinates and structure factors have been deposited in the RCSB Protein Data Bank (access code 3COH).

* To whom correspondence should be addressed. Phone: 650-225-5943. Fax: 650-225-3734. E-mail: andrea@gene.com.

[†] Department of Small Molecule Drug Discovery, Genentech, Inc.

[‡] Department of Medicinal Chemistry, Roche Diagnostics GmbH.

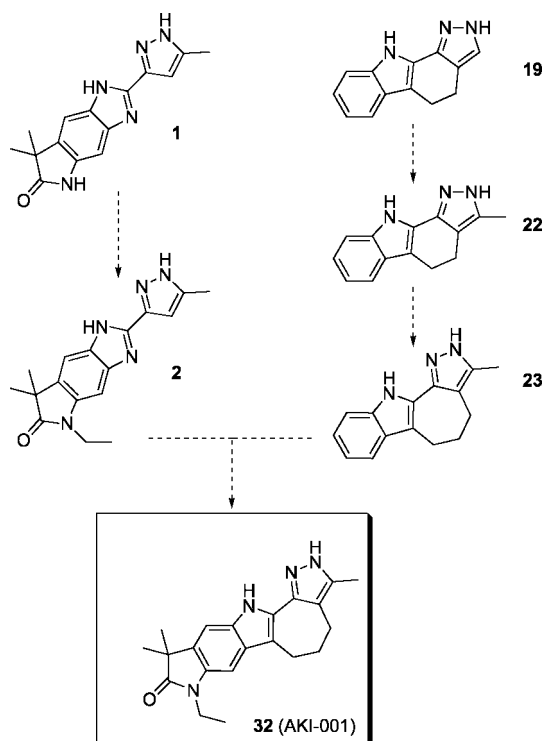
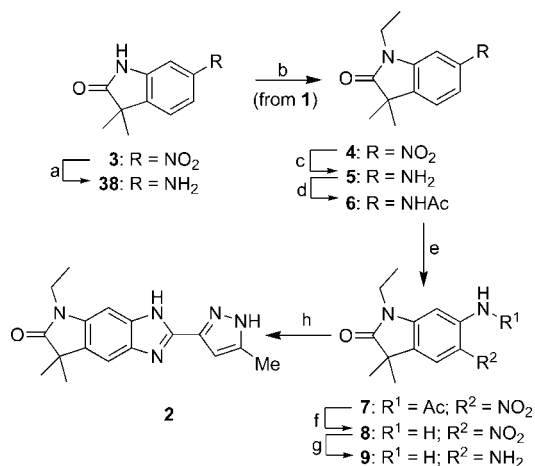
[§] Department of Translational Oncology, Genentech, Inc.

[#] Department of Cell Cycle and Global Regulators, Genentech, Inc.

[⊥] Department of Cell Biology, Roche Diagnostics GmbH.

^{||} Department of HTS and Biochemistry, Roche Diagnostics GmbH.

[∇] Department of Protein Engineering, Genentech, Inc.

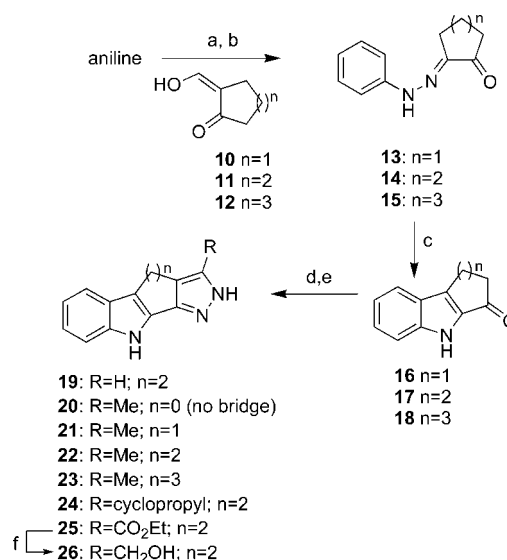
Scheme 1. Progression and Combination of Benzimidazole (Left) and Tetracycle (Right) Lead Series**Scheme 2.** General Synthesis of Benzimidazoles^a

^a (a) H₂, Pd/C; (b) NaH, EtBr; (c) H₂, Pd/C; (d) Ac₂O; (e) Ac₂O, HNO₃, (f) HCl; (g) H₂, PtO₂; (h) 5-methyl-1*H*-pyrazole-3-carboxylic acid, polyphosphoric acid, P₂O₅, heat.

with excellent oral availability and very potent activity in mouse xenograft models.

Chemical Synthesis

The synthesis of benzimidazole **1** has been described.^{33,34} The conceptually parallel synthesis of the ethyl analogue **2** is outlined in Scheme 2. Treatment of 6-nitrolactam **3**³³ with NaH and bromoethane yielded *N*-ethyl lactam **4**. Hydrogenation of the nitro group, followed by acylation of resulting aniline **5**, yielded the protected intermediate **6** in 78% overall yield for the three steps. Nitration of **6** in a mixture of acetic anhydride and nitric acid gave the 5-nitro derivative **7** in good yield (78%). Hydrolysis of the acetamide followed by hydrogenation of nitroaniline **8** yielded the 5,6-diamino intermediate **9** in 83%

Scheme 3. General Synthesis of Tetracyclic Core^a

^a (a) NaNO₂, HCl, H₂O, cold; (b) **10**, **11**, or **12**; NaOAc; H₂O/MeOH; (c) HCl, HOAc, heat; (d) DMFDMA (R = H) or [(CH₃)₃Si]₂NLi, electrophile, THF; (e) N₂H₄, EtOH; (f) LiAlH₄, THF.

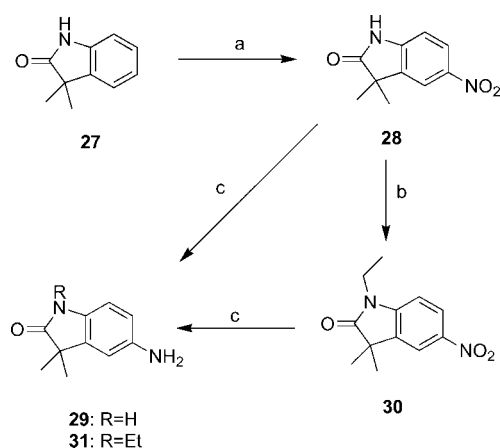
overall yield from **7**. Condensation of **9** with the appropriate pyrazole carboxylic acid gave the final product **2** in 20% yield after purification.

Construction of the tetracyclic core (Scheme 3) began with nucleophilic addition of the appropriate β -ketoaldehyde (**10–12**)^{35–37} to anilino diazonium chloride generated in situ, producing, in a Japp–Klingemann reaction, **13–15** in 43–92% yield. Subsequent Fischer cyclization under warm acidic conditions gave the corresponding ketoindoles **16–18**^{38–40} in 64–77% yields. The unsubstituted pyrazole analogue **19** was formed by thermal condensation of **17** with *N,N*-dimethylformamide dimethylacetal and hydrazine to give the desired product in 11% yield. 5-Methylpyrazole analogues **20–23** were prepared from enolates obtained by treatment of either commercially available 2-acetylindole (for the acyclic analogue **20**) or cyclic compounds **16–18** with lithium bis(trimethylsilyl)amide. Electrophilic addition of acetic anhydride followed by immediate reaction of the β -diketone intermediates with hydrazine then gave compounds **20–23** in 7–24% yield. The electrophiles cyclopropanoyl chloride and diethyl oxalate were used in analogous fashion to generate compounds **24** and **25** in 47% and 54% yields, respectively. Reduction of **25** with LAH gave compound **26** in 75% yield.

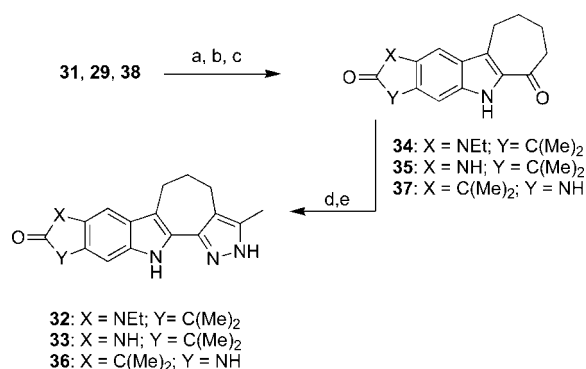
Synthesis of the pentacyclic series required the 5-amino regioisomer of lactam **5**. Regioselective nitration of 1,3-dihydro-3,3-dimethyl-2*H*-indol-2-one⁴¹ (**27**) was accomplished in 63% yield (Scheme 4). Nitrolactam **28** was either directly reduced (H₂, Pd/C) to afford the aniline **29** or, alternatively, ethylated before reduction to afford **31**. Synthesis of pentacycles **32** and **33** then proceeded as described above for the tetracycles via keto intermediates **34** and **35**, respectively (Scheme 5). Synthesis of analogue **36** proceeded likewise via **37**, synthesized from aniline **38** (Scheme 2).

Results and Discussion

We undertook a screening campaign against Aurora A kinase to identify promising lead compounds. Among the initial screening hits were the related structures **1** and **19** (Scheme 1). Upon being retested, these compounds exhibited modest IC₅₀ values of 0.18 and 0.30 μ M, respectively, in an Aurora A

Scheme 4. Construction of Lactam^a

^a (a) Fuming HNO₃, H₂SO₄; (b) NaH, EtBr; (c) H₂, Pd/C.

Scheme 5. Completion of Pentacycles^a

^a (a) NaNO₂, HCl, H₂O, cold; (b) **12**, NaOAc, H₂O/MeOH; (c) HCl, HOAc, heat; (d) [(CH₃)₃Si]₂NLi, Ac₂O, THF; (e) N₂H₄, EtOH.

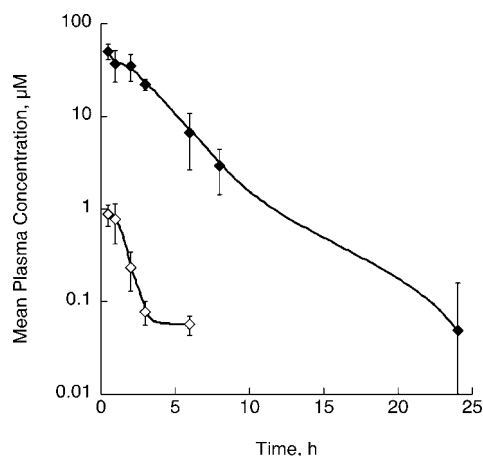


Figure 1. Comparison of pharmacokinetics of compounds **1** (open symbols) and **2** (closed symbols) after oral dosing (30 mg/kg) in mouse. Compounds were formulated as suspensions in gelatin.

enzymatic assay. However, cellular potency was relatively poor for compound **1** (5–20 µM against several cell lines) and undetectable for compound **19** (>20 µM). Pharmacokinetic studies in mouse gave promising results for compound **19**, which showed significant oral bioavailability and a moderate rate of clearance (not shown), whereas compound **1** was cleared rapidly and exhibited a low C_{max} after oral dosing (Figure 1). We therefore undertook a preliminary SAR investigation of com-

Table 1. Lactam Analogues of Compound **1**

R	AurA IC ₅₀ , µM	AurB IC ₅₀ , µM	C _{max} , µM	AUC _{last} , h µM
1 H	0.18	0.15	0.88	1.5
2 Et	0.069	0.13	51	180

Table 2. Pyrazole Analogues of Compound **19**

R	AurA IC ₅₀ , µM
19 H	0.30
22 Me	0.051
24 cyclopropyl	0.11
25 COOEt	5.7
26 CH ₂ OH	0.34

Table 3. Bridging Ring Analogues of Compound **22**

n	AurA IC ₅₀ , µM	AurB IC ₅₀ , µM	HT29 IC ₅₀ , µM	MCF7 IC ₅₀ , µM
20 0 ^a	1.1	0.51	nd ^b	nd ^b
21 1	0.87	0.88	>20	>20
22 2	0.051	0.22	>20	4.5
23 3	0.042	0.022	2.6	0.67

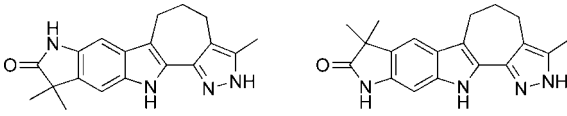
^a No bridge. ^b Not determined.

pounds **1** and **19**, with the particular goal of improving cellular potency and oral exposure.

Exploration of the lactam portion of compound **1** (Table 1) revealed that N-alkylation had little effect on enzymatic potency and modestly improved cellular potency (~10-fold, not shown). However, this modification, especially N-ethylation, had a profound effect on oral PK properties (Figure 1). By comparison of the N-ethyl analogue **2** to the parent **1**, C_{max} increased by a factor of 57 while AUC_{last} increased 117-fold. Other N-alkyl lactam derivatives explored showed improvement relative to **1**, but none had properties as favorable as **2** (not shown).

Our investigation of the tetracycle **19** began with an assessment of the effects of substitution on the pyrazole. On the basis of structures of reported Aurora inhibitors (and, in particular, the structure of compound **1**), we introduced a group of relatively small substituents at position 5 of the pyrazole ring (Table 2). Analogues containing hydrophilic or sterically demanding groups showed a decrease in activity (examples **25** and **26**), while the relatively small and lipophilic methyl substitution (**22**) appeared to optimize potency. Accordingly, the methylpyrazole was fixed in subsequent analogues.

We then explored the role of the hydrocarbon bridge joining the pyrazole to the indole and varied its length (Table 3). As expected, the lack of a constraining ring significantly reduced potency compared to the six-membered ring present in compounds **19** and **22**. However, we found that expansion to a seven-membered ring appeared slightly beneficial, particularly

Table 4. Exploration of Lactam Orientation


	33		36	
	AurA IC ₅₀ , μM	AurB IC ₅₀ , μM	HT29 IC ₅₀ , μM	MCF7 IC ₅₀ , μM
33	0.0020	<0.002	0.030	0.10
36	0.072	0.086	2.6	1.5

Table 5. Activities of **32** and Its Parents in Various Assays

values in μM	2	23	32	39^b
IC ₅₀ , Aurora A	0.069	0.042	0.004	0.006
IC ₅₀ , Aurora B	0.13	0.022	0.005	0.030
IC ₅₀ , HCT116	3.3	nd ^a	0.070	0.053
IC ₅₀ , HT29	4.3	2.6	0.070	0.15
IC ₅₀ , MCF7	2.1	0.67	0.10	0.048
G2/M block	2.2	2.2	0.11	nd ^a
p-Aurora A, HCT116	3.9	10	0.16	0.31
centrosome separation, HCT116	1.3	5.0	0.08	0.31
p-histone H3, HT29	6.6	6.6	0.10	0.74
p-histone H3, HCT116	nd ^a	10	0.31	0.31

^a Not determined. ^b Previously described pan-Aurora inhibitor²⁷ included as a positive control.

when assayed against Aurora B (compound **23**). Gratifyingly, in addition to this improvement in enzymatic potency, **23** was significantly improved in cellular potency.

After limited optimization, our two lead series had improved in certain target properties, namely, oral availability for benzimidazole **2** and measurable cellular potency for tetracycle **23**. Nevertheless, potency (enzymatic and cellular) was still rather less than we desired. We were intrigued by the structural similarity between the two series. Each has a “donor–acceptor–donor” arrangement of hydrogen-bonding groups frequently seen in kinase inhibitors that bind to the adenine-binding “hinge” region of the ATP-binding pocket, and it seemed likely that these would be critical affinity determinants. It also appeared that both the hydrocarbon bridge of **23** and the lactam portion of **2** contributed favorably to binding (compare **20** to **23** and **20** to **2**; Tables 3 and 1). We therefore decided to merge **2** and **23** into a single pentacyclic analogue **32** (AKI-001, Scheme 1). Two orientations of the lactam ring are possible. Our decision to orient the ring as in **32** was based on comparison of the related des-ethyl compounds **33** and **36** (Table 4).

Inclusion of both the lactam ring and the hydrocarbon constraint in **32** led to an increase in enzymatic potency of ~10-fold compared to **2** and **23** (Table 5). The binding mode was determined from a 2.7 Å X-ray cocrystal structure (Figure 2). As expected, the indole and pyrazole nitrogens arrayed along the edge of **32** participate in hydrogen-bonding interactions with the amide backbone of the Aurora A hinge region (Figure 2A). The methylpyrazole occupies the back of the ATP pocket, where it is rather tightly accommodated and binds in the same orientation seen for the methylpyrazole of **39** (Chart 1) in complex with a Gleevec-resistant mutant (His396Pro) of Abl kinase (PDB code 2F4J, Figure 2B).⁴² The pyrazole pocket is defined in part by the Aurora A “gatekeeper” residue Leu210, which appears to block access from the pyrazole methyl group to a deeper hydrophobic pocket, consistent with the observed preference for small pyrazole substituents (Table 2). The lactam portion of **32** extends toward solvent and overlays the solubilizing methylpiperazine of **39**.

One difference between the two cocrystal structures is the conformation of the conserved Asp residue in the “DFG” motif

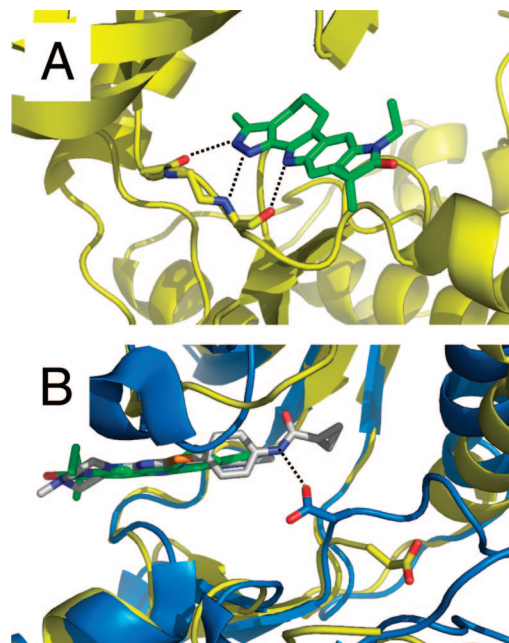
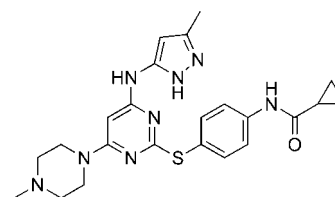


Figure 2. Comparison of cocrystal structures of **32** bound to Aurora A and the Aurora kinase inhibitor **39** bound to mutant Abl kinase (PDB code 2F4J⁴²): (A) hydrogen bonds between **32** (shown in green) and the “hinge” region in the ATP-binding pocket of Aurora A; (B) comparison of orientation of the conserved Asp residue at the beginning of the activation loop for Abl (blue) bound to **39** (white) and Aurora A bound to **32** (same color scheme as in part A).

Chart 1. Structure of the Pan-Aurora Kinase Inhibitor **39** (VX-680)²⁷



at the beginning of the activation loop. In the **39**/Abl structure, the side chain Asp381 points in toward the active site and forms a hydrogen bond with the NH of the cyclopropylamide of **39**. This “DFG-in” orientation of Asp381 is consistent with an activated conformation of the kinase and differs from that observed when Gleevec is bound to wild-type Abl.⁴² Binding of Gleevec instead causes the side chain of Asp381 to rotate away from the active site and an associated reorientation of Phe382, leading to the so-called “DFG-out” inactive conformation of Abl. In the complex structure of **32** bound to Aurora A, a segment of the activation loop is disordered (residues 275–288). The lack of order in this loop may be influenced by the mutation of the phosphorylation sites T287 and T288 to alanine. Nevertheless, Asp274 would appear to adopt the “DFG-out” orientation (Figure 2B), suggesting that **32** can bind to an inactive conformation of Aurora A.

32 was greatly improved in antiproliferative activity against several tumor cell lines (Table 5). This antiproliferative effect coincided with the compound concentration required to produce a G2/M block (24 h assay), as measured by flow cytometry. We used several more specific cellular assays to judge whether the observed antiproliferative effect was driven by inhibition of Aurora A, Aurora B, or both (Figure 3). For inhibition of Aurora A, we used two cellular readouts in the HCT116 colon cancer cell line: loss of autophosphorylation of Aurora A at

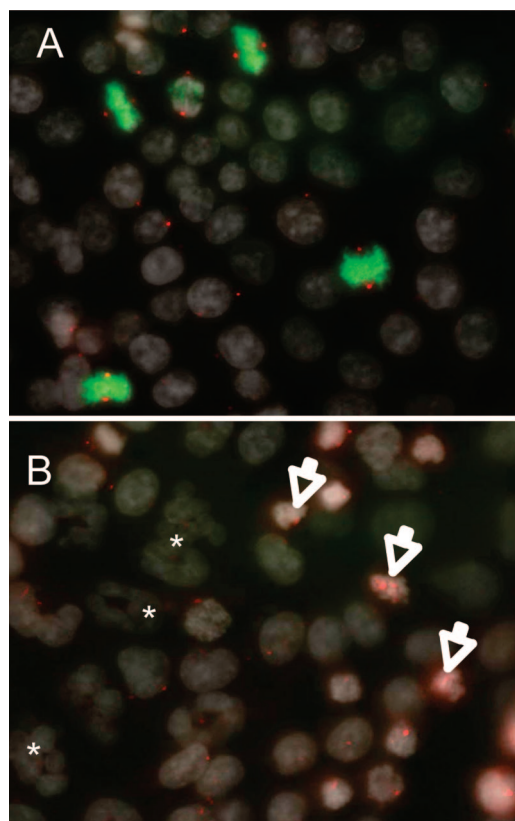


Figure 3. Cellular effects of **32**. HCT116 cells were incubated with (A) DMSO or (B) 100 nM **32** for 16 h, then fixed and stained for phosphohistone H3 (Ser10) (green), Aurora A (red), and DNA (gray). Note that inhibitor-treated mitotic cells (arrows) have poorly separated centrosomes, indicating inhibition of Aurora A, and fail to stain for phosphohistone H3, indicating inhibition of Aurora B. After ~2 h, these aberrant mitotic cells undergo chromatin decondensation, forming multilobed nuclei (indicated by an asterisk).

Thr 288 and failure of centrosomes to separate. These occurred with thresholds for complete inhibition at 0.16 and 0.08 μM **32**, respectively. To assess inhibition of Aurora B, we determined the threshold for complete loss of phosphohistone H3 staining in mitotic cells. This effect was seen at 0.31 μM in the HCT116 cell line and at 0.10 μM in the colon cancer line HT29. Overall, **32** is approximately equipotent in cellular inhibition of Aurora A and Aurora B (consistent with the equivalent enzymatic IC_{50} values), and the compound concentrations required to produce these effects are fairly close to the antiproliferative IC_{50} values. This suggests that the antiproliferative effect is likely to be a consequence of Aurora inhibition. To explore this further, we assayed **32** in a panel of kinase assays (Table 6 and Supporting Information Table S2). Importantly, there is little inhibition of non-Aurora kinases important for cell cycle progression (for example, CDK or PLK family members). However, **32** does show off-target activities, most notably against receptor tyrosine kinases and Src family members as has been reported for other Aurora kinase inhibitors.^{27,30,42}

There has been much discussion in the literature of the dominance of Aurora B inhibition phenotypes over those of Aurora A. We can clearly see both effects in the short inhibitor exposure times (~60 min) necessary for the immunofluorescence assays. (Similar observations of dual inhibition have recently been reported for cells treated with **39**.⁴³) Over the longer exposure times needed for antiproliferative assays (4–5 days), we see extensive polyploidization similar to that previously reported for Aurora A/B inhibitors. This is consistent with a

Table 6. Kinase Selectivity of **32**

kinase	IC_{50} , μM^a	% activity at 1 μM^b
CDK2/cyclinA	15	
CDK3/cyclinE		106
CDK5/p25		8
CDK6/cyclinD3		103
CDK7/cyclinH/MAT1		82
CDK9/cyclinT1		87
Chk1	0.085	
NEK2		98
Plk3		103
Abl		10
Flt3	0.002	
GSK3 β	7.7	
KDR	0.012	
Src	0.25	
TrkB		2

^a IC_{50} determination in-house at [ATP] = K_m . ^b Single point activity determinations from a commercial selectivity panel (Upstate; 100% corresponds to no inhibition of the target enzyme).

failure of cytokinesis from inhibition of Aurora B. It is difficult to assess the relative contributions of Aurora A and Aurora B inhibitory activities to the block in cellular proliferation, but it is clear that with **32**, an early mitotic block cannot be maintained indefinitely; eventually cells bypass the spindle checkpoint, likely through inhibition of Aurora B, and undergo endoreplication (repeated replication of DNA without cell division).

Given the improvements in potency we observed for **32**, we decided to evaluate it further in vivo (Figure 4). Pentacycle **32** showed significant and sustained exposure after a single oral dose of 5 mg/kg in mouse, exceeding the threshold required for cellular inhibition (~0.1 μM) for at least 10 h (Figure 4A). Oral exposure was evaluated also in rat and dog (Table 7) and found to be significant. We therefore tested the efficacy of **32** in an HCT-116 mouse xenograft model. Substantial inhibition of tumor growth was observed for QD doses of 2.5 (82% TGI; $p < 0.0001$) and 5 mg/kg (92% TGI; $p < 0.0001$), while a lesser effect was observed at the 1 mg/kg dose (52% TGI; $p = 0.0002$) (Figure 4B). The compound was well tolerated at 1, 2.5, and 5 mg/kg doses, as judged by minimal loss of body weight (Figure 4C), while dosing at 10 mg/kg QD led to unacceptable weight loss, marked bone marrow depletion, and gastrointestinal hypocellularity. These effects are similar to those observed with other Aurora inhibitors and antimetabolic agents generally.

Conclusion

Pentacycle **32** represents a new class of pan-Aurora kinase inhibitors with excellent oral availability and high potency against tumor xenografts in mouse. These properties compare favorably with those of other reported Aurora kinase inhibitors. Cellular studies support Aurora kinase inhibition as the mechanism of antiproliferative activity and, presumably, of tumor growth inhibition.

Experimental Section

Expression and Purification of Aurora Kinases. Both Auroras A and B were cloned into pET21a (EMD Biosciences) and expressed in BL21-DE3 pLysS-Rosetta (EMD Biosciences). Transformants were grown with shaking at 37 °C in LB broth supplemented with 50 $\mu\text{g}/\text{mL}$ carbenicillin and 12.5 $\mu\text{g}/\text{mL}$ chloramphenicol until cultures reached an A_{600} reading of 0.45–0.6. Expression was induced with 0.4 mM isopropyl- β -D-1-thiogalactopyranoside (IPTG), and the cultures were transferred to a shaker at room temperature (~18–22 °C) for an additional 12–16 h. The construct for Aurora A kinase domain surrogate included residues 124–391 with the following amino acid substitutions: K124A, K153R, V206I, R251K, L289M, and K339R. Aurora B surrogate

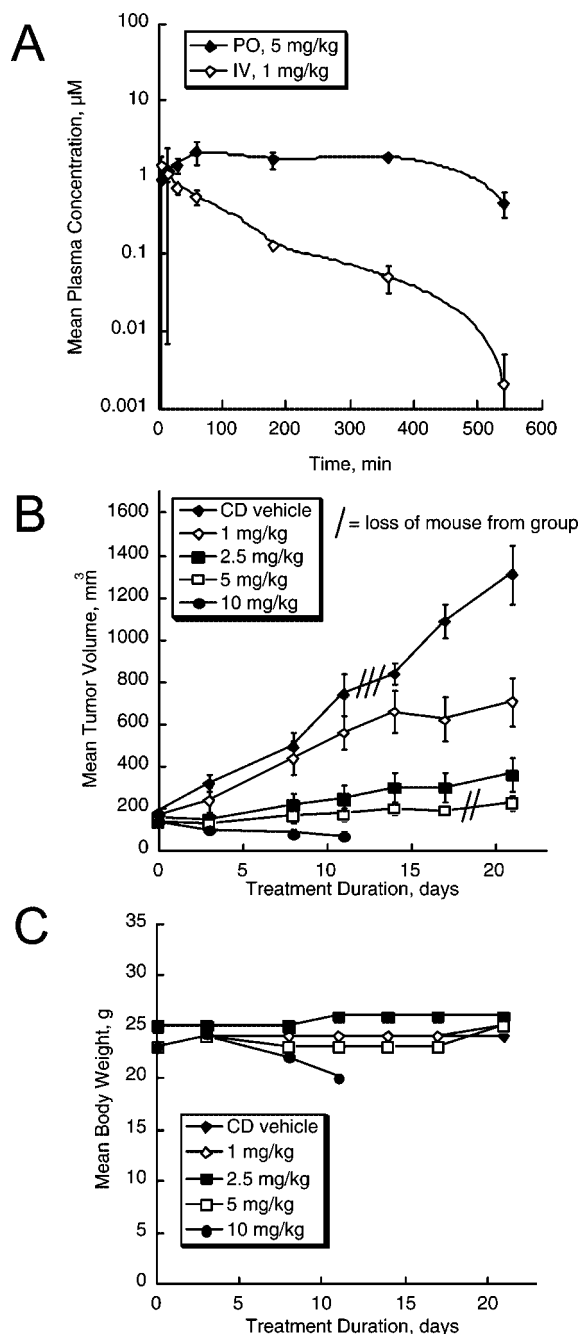


Figure 4. In vivo evaluation of **32**: (A) pharmacokinetics after dosing orally (po, 5 mg/kg, closed symbols) or intravenously (iv, 1 mg/kg, open symbols); (B) tumor growth in an HCT116 xenograft model at 0, 1, 2.5, 5, and 10 mg/kg daily (QD) oral doses of **32**. (Five mice were terminated during study; see Experimental Section.) (C) Body weight of mice in the xenograft study shown in part B.

was N-terminally FLAG-tagged (Sigma) full length protein with the following amino acid substitutions: S61K, K97R, I150V, M233L, K195R, R283K. All substitutions were at solvent-exposed sites well away from the ATP-binding pocket. Specific activities of the mutant proteins (in the assays described below) were indistinguishable from those of wild-type (see Figure S1). The construct of Aurora A used for crystallography was the same as that described above but with the substitutions K124A, Q154N, A203S, R251K, T287A, T288A, and E336D.

Purification of both Auroras was facilitated after we observed that they were retained on Ni-NTA columns despite lacking His₆ tags. All purification steps were performed at 4 °C. Frozen cell pellets were thawed and resuspended in 20 mM HEPES, pH 7.5, 0.5 M NaCl, 20% v/v glycerol, 5 mM β-mercaptoethanol (β-ME).

Table 7. Pharmacokinetic Properties of **32**

species	CL, mL min ⁻¹ kg ⁻¹ ^a	F, ^b %
mouse	25	178
rat	22	97
dog	34	56

^a Formulation of iv dosing solutions differs in each case and is given (along with additional details) in the Experimental Section. ^b Oral dosing was performed in all cases with solutions of **32** in 80% polyethylene glycol.

After the sample was passed through a microfluidizer, lysates were centrifuged for 30 min at 10 000 rpm. Supernatant was then loaded on Ni-NTA Superflow resin (Qiagen) previously equilibrated in lysis buffer. The column was washed with 4 × 8 column volumes of lysis buffer containing 5 mM imidazole. Kinase was eluted with 0.5 M imidazole, pH 7.0, 0.5 M NaCl, 20% v/v glycerol, 5 mM β-ME, either in a step fashion (4 × 1 column volume) or by linear gradient from wash buffer for larger scale work.

Aurora A was further purified by dilution with 20 mM HEPES, pH 7.5, 5 mM EDTA, 20% v/v glycerol, 5 mM dithiothreitol (DTT) to a final NaCl concentration of 50 mM. This solution was loaded onto an SP Sepharose fast flow column (GE Healthcare) previously equilibrated in dilution buffer. After the sample was washed with the same buffer, kinase was eluted in a linear gradient from 0.05 to 0.5 M NaCl in dilution buffer over 5 column volumes. Final purification of the Aurora A for crystallography was performed on a Superdex 75 column (26/60, GE Healthcare) equilibrated in 0.5 M NaCl, 20 mM HEPES, pH 7.2, 20% v/v glycerol, 5 mM DTT, 1 mM EDTA. Purity was assessed by SDS-PAGE. Mass spectrometry confirmed that Aurora A isolated from *E. coli* was autophosphorylated and that the major species contained two phosphates. Subsequent peptide mapping identified Thr277 and Thr288 as the major autophosphorylation sites (not shown), consistent with published observations.⁴⁴

Aurora B fractions eluted from the Ni column were combined and loaded onto anti-FLAG M2 agarose (Sigma) previously equilibrated in lysis buffer lacking β-ME. The column was washed with 6 × 2.5 column volumes of the same buffer. Kinase was then eluted with FLAG peptide (Sigma; 100 µg/mL in the same buffer, 5 × 0.75 column volumes). The most concentrated fractions of highly purified Aurora B were identified by SDS-PAGE and combined. Like Aurora A, Aurora B was purified in active form from *E. coli*, albeit at ~10-fold lower yield because of its limited solubility.

Crystallography. Aurora A was desalted prior to crystallization using a NAP 5 column (Amersham) equilibrated with 40 mM HEPES, pH 7.2, 50 mM NaCl, 5 mM DTT. The final concentration of protein was 20 mg/mL. Inhibitor stock (20 mM) was prepared in DMSO. The compound was added to Aurora A at a final concentration of 0.1 mM and incubated on ice for 30 min. Crystallization was carried out using sitting drops containing an equal volume of complex plus reservoir. The reservoir contained 30% w/v PEG 3350, 0.2 M ammonium acetate, and 0.1 M HEPES, pH 7.5. Crystals appeared within 3–4 days at 18 °C and grew to 0.1 mm × 0.1 mm × 0.1 mm within a week.

Data were collected at the Stanford Synchrotron Radiation Laboratory and processed using Denzo and Scalepack from the HKL Suite.⁴⁵ Crystals contained two molecules in the asymmetric unit; cell parameters and data statistics are summarized in Supporting Information Table 1. The structure was solved by molecular replacement using AmoRe⁴⁶ using the coordinates of 1MUO (RCSB Protein DataBank) as a search model. Model building and refinement were performed using the programs O⁴⁷ and Refmac,⁴⁸ respectively.

Inhibition Assays. Both Auroras A and B were assayed in ELISA format using a GST fusion (pGEX-4T, GE Healthcare) of the N-terminus of Histone H3 (aa 1–18) as substrate. Plates were coated with 2 µg/mL substrate in PBS then blocked with 1 mg/mL I-block (Tropix) in PBS. Kinase reactions were run for 40 min with 5 ng/mL (0.16 nM) Aurora A or 45 ng/mL (1.1 nM) Aurora B at 30 µM ATP (~K_m) in kinase buffer (Cell Signaling). Final DMSO

concentration was 4%. Product was detected by incubation with antiphosphohistone H3 (Ser10) 6G3 mouse monoclonal antibody (Cell Signaling, 1:4000) and sheep-antimouse HRP conjugate (Amersham, 1:4000), followed by washing and addition of TMB substrate (Kirkegaard & Perry Laboratories). After quenching with 1 M phosphoric acid, plates were read at 450 nM.

Cell-Based Antiproliferative Assays. Inhibitors were tested for activity against the human colon cancer cell lines HCT116 and HT29 and against the human breast cancer cell line MCF7. Cells were seeded in 384-well plates on day 0 in 50 μ L of complete medium (1:1 mixture of Ham's F12 and DMEM-high glucose supplemented with 10% fetal bovine serum and 2 mM L-glutamine) and incubated overnight in a 5% CO₂ atmosphere at 37 °C. On day 1, 10 μ L of diluted inhibitor (DMSO solution of desired concentration diluted 20-fold with the above medium lacking serum and glutamine) was added to cells. Cells were incubated as described above. On day 4, plates were allowed to reach room temperature, and 30 μ L Cell Titer-Glo reagent (Promega) was added to each well (to measure total ATP levels). Plates were read after shaking 15 min at room temperature.

Cell-Cycle Analysis. Human MOLT-4 leukemia cells were treated with 3-fold serial dilutions of inhibitors for 24 h at 37 °C. Cells were collected by centrifugation and resuspended in 0.1 M Tris, pH 7.4, 154 mM NaCl, 1 mM CaCl₂, 0.5 mM MgCl₂, 0.2% bovine serum albumin, 0.1% Nonidet P 40. Resuspended cells were treated on ice for 30 min with 60 U/mL RNase A (Calbiochem) and 20 μ g/mL propidium iodide (Sigma). DNA content was then determined by FACS.

Aurora A and Aurora B Phenotypic Assays. HCT116 or HT29 cells were treated with 2-fold serial dilutions of inhibitors for 4 h, fixed with 4% paraformaldehyde, permeabilized with 0.2% Triton X-100, and stained with the antibodies indicated below. Slides were then imaged on the high-content screening ImageXpress system and quantitated in MetaXpress software (Molecular Devices). Approximate threshold concentrations for complete failure of centrosome separation and loss of phospho-Aurora A staining served to estimate Aurora A inhibition in cells. Approximate concentrations for the complete loss of phosphohistone staining of mitotic cells (MPM2 positive cells) served to estimate Aurora B inhibition in cells.

Primary antibodies used include total Aurora A (Santa Cruz, SC-14321; 1:500 dilution), phospho-Aurora A (Cell Signaling, 3091; 1:350 dilution), MPM2 (Upstate, 05-368; 1:4000 dilution), and phosphohistone H3 (serine 10) (Cell Signaling, 9701; 1:350 dilution).

Pharmacokinetics Evaluation of 32. For the mouse study shown in Figure 4A, three female CD-1 mice were dosed for each time point. For iv dosing (1 mg/kg), drug was formulated as a solution in 5% DMSO, 5% Cremophor. For po dosing (5 mg/kg), the drug was given as a solution in 80% polyethylene glycol (PEG). For the rat study, three male SD rats were dosed per route. The po dosing was as described above for mouse, and the iv dose (1 mg/kg) was also administered as an 80% solution in PEG. For the dog study, three male beagles were dosed per route. Again, oral dosing was as described above for mouse, while the iv dose (1 mg/kg) was delivered as a solution in 60% PEG. Averages of serum levels ($N = 3$) were used to calculate PK parameters.

In Vivo Efficacy Study. For the HCT-116 xenograft study, female athymic nude mice were injected subcutaneously in the right flank with 5×10^6 cells. When tumors reached a mean volume of ~ 150 mm³, mice with near average-sized tumors were randomly assigned to groups ($N = 10$) for dosing. **32** was formulated as a suspension in 20% HP- β -cyclodextrin. Mice were dosed orally QD with 100 μ L of vehicle containing the appropriate dose of inhibitor (0, 1, 2.5, 5, or 10 mg/kg). Three mice from each group were sacrificed for PD analysis after 2 days of dosing; the remainder were dosed for 21 days. Mice were euthanized if tumors became excessively large (≥ 2000 mm³) or if 20% of body weight was lost. Significance (p -value) of observed differences in average end-of-study tumor volumes was calculated using Dunnett's method. Percent tumor growth inhibition (% TGI) was calculated

from the ratio of the change in average tumor volumes for **32** vs vehicle treatment: $TGI = 100(1 - [(V_{day21} - V_{day0})_{dose} / (V_{day21} - V_{day0})_{vehicle}])$.

General Synthetic Procedures. All reactions were carried out under a nitrogen atmosphere with dry solvents under anhydrous conditions, unless otherwise noted. Reagents were purchased at the highest commercial quality available and were used without further purification unless otherwise stated. Reactions were monitored by thin-layer chromatography (TLC) carried out on 0.25 mm E. Merck silica gel plates (60F-254) using UV light as visualizing agent. Alternatively, an ethanolic solution of phosphomolybdic acid or cerium sulfate, followed by heating, was used as a developing agent. E. Merck silica gel 60 (particle size 0.040–0.063 mm) was used for flash column chromatography. NMR spectra were recorded on Varian 400 instruments and were calibrated using chemical shifts of residual undeuterated solvent. The following abbreviations were used to explain the multiplicities: s = singlet, d = doublet, t = triplet, q = quartet, m = multiplet, br = broad. Electrospray ionization (ESI) mass spectrometry (MS) experiments were performed on an API100 Perkin-Elmer SCIEX single quadrupole mass spectrometer at 4000 V emitter voltage. Yields refer to chromatographically and spectroscopically (¹H NMR) homogeneous materials, unless otherwise stated.

7,7-Dimethyl-2-(5-methyl-1H-pyrazol-3-yl)-6-oxo-1H-imidazo[4,5-f]indole (1). Compound **1** was synthesized as described.^{33,34} HPLC purity 99.8%.

1-Ethyl-3,3-dimethyl-6-nitroindol-2-one (4). A solution of **3**³³ (6 g, 29.10 mmol) in anhydrous *N,N*-dimethylformamide (DMF, 35 mL) was treated with sodium hydride (0.9 g, 37.8 mmol). The resulting suspension was stirred for 1 h at 60 °C. A solution of bromoethane (2.17 mL, 3.17 g, 29.10 mmol) in DMF (10 mL) was added. The mixture was allowed to cool to room temperature and stirred for 1 h. After removal of solvent, the mixture was quenched with water (100 mL) and extracted with ethyl acetate (3 \times 100 mL). The extract was dried over Na₂SO₄ and evaporated, and the crude product was purified by column chromatography on silica gel. Elution with ethyl acetate/*n*-heptane (1:3) yielded 5.94 g (87%) as a yellow solid. MS (ESI+) $m/z = 235.3$ ($M + 1$); ¹H NMR (400 MHz, DMSO-*d*₆) δ 7.97 (d, $J = 8.3$ Hz, 1H), 7.86 (s, 1H), 7.66 (d, $J = 8.3$ Hz, 1H), 3.81 (q, $J = 7.0$ Hz, 2H), 1.32 (s, 6H), 1.16 (t, $J = 7.0$ Hz, 3H).

6-Amino-1-ethyl-3,3-dimethylindol-2-one (5). To a solution of **4** (5.9 g, 25.19 mmol) in methanol/tetrahydrofuran (THF) (1:1, 80 mL) palladium on charcoal (10%, 1.2 g) was added, and the mixture was hydrogenated at ambient pressure and room temperature for 4 h. After filtration and evaporation of the solvents, 5.05 g (98%) of **5** was isolated as a white solid. MS (ESI+) $m/z = 205.0$ ($M + 1$); ¹H NMR (400 MHz, DMSO-*d*₆) δ 6.92 (d, $J = 7.8$ Hz, 1H), 6.25 (s, 1H), 6.21 (d, $J = 7.8$ Hz, 1H), 5.12 (br, 2H), 3.58 (q, $J = 7.1$ Hz, 2H), 1.17 (s, 6H), 1.11 (t, $J = 7.1$ Hz, 3H).

6-Acetamido-1-ethyl-3,3-dimethylindol-2-one (6). A solution of **5** (5.05 g, 24.72 mmol) in acetic anhydride (80 mL) was stirred at room temperature for 4 h. The mixture was poured into ice–water (150 mL), allowed to warm to room temperature, and was stirred again for 2 h. After extraction with ethyl acetate (3 \times 100 mL), the combined organic layers were washed with saturated NaHCO₃ solution (3 \times 100 mL) and brine (100 mL), then dried over sodium sulfate. After removal of solvent, the crude product was purified by column chromatography on silica gel (ethyl acetate/*n*-heptane 1:1) yielding 5.6 g (91%) of **6** as a light-yellow solid. MS (ESI+) $m/z = 247.1$ ($M + 1$); ¹H NMR (400 MHz, DMSO-*d*₆) δ 9.97 (br, 1H), 7.37 (s, 1H), 7.23 (d, $J = 8.0$ Hz, 1H), 7.12 (d, $J = 8.0$ Hz, 1H), 3.63 (q, $J = 7.1$ Hz, 2H), 2.04 (s, 3H), 1.23 (s, 6H), 1.13 (t, $J = 7.1$ Hz, 3H).

6-Acetamido-1-ethyl-3,3-dimethyl-5-nitroindol-2-one (7). To a solution of **6** (5.6 g, 22.73 mmol) in acetic anhydride (70 mL) at 0 °C, nitric acid (100%, 1.96 g, 1.29 mL, 31.2 mmol) was added. The mixture was stirred for 30 min, then poured onto ice–water (150 mL). After being stirred for 4 h, the mixture was extracted with ethyl acetate (3 \times 100 mL). The combined organic layers were washed with sodium hydroxide solution (1 M, 100 mL) and

water (100 mL), dried over sodium sulfate, and concentrated. The crude product was purified by column chromatography on silica gel (ethyl acetate/*n*-heptane 1:1) to yield 5.2 g (78%) **7** as a yellow solid. MS (ESI+) $m/z = 292.0$ ($M + 1$); $^1\text{H NMR}$ (400 MHz, DMSO- d_6) δ 10.39 (br, 1H), 8.12 (s, 1H), 7.54 (s, 1H), 3.71 (m, 2H), 2.13 (s, 3H), 1.31 (s, 6H), 1.16 (t, $J = 7.1$ Hz, 3H).

6-Amino-1-ethyl-3,3-dimethyl-5-nitroindol-2-one (8). Compound **7** (5.2 g, 17.85 mmol) was dissolved in ethanol (80 mL). After addition of hydrochloric acid (25%, 8 mL, 81.44 mmol), the mixture was stirred under reflux for 3 h. The reaction mixture was allowed to cool to room temperature and then was quenched with water (80 mL). A yellow precipitate was isolated by filtration and washed with ethanol/water (1:1). The solid was dissolved in ethyl acetate, dried over sodium sulfate, and concentrated to yield 4.15 g (93%) of **8** as an orange solid. MS (ESI+) $m/z = 250.0$ ($M + 1$); $^1\text{H NMR}$ (400 MHz, DMSO- d_6) δ 7.95 (s, 1H), 7.67 (br, 2H), 6.54 (s, 1H), 3.64 (m, 2H), 1.27 (s, 6H), 1.15 (t, $J = 7.1$ Hz, 3H).

5,6-Diamino-1-ethyl-3,3-dimethylindol-2-one (9). To a solution of **8** (4.15 g, 16.65 mmol) in ethanol (80 mL), PtO₂ (0.4 g) was added and the mixture hydrogenated at ambient pressure and room temperature for 3.5 h. After filtration and evaporation of solvent, 3.25 g (89%) of **9** was isolated as an orange solid. MS (ESI+) $m/z = 220.0$ ($M + 1$); $^1\text{H NMR}$ (400 MHz, DMSO- d_6) δ 6.50 (s, 1H), 6.27 (s, 1H), 4.48 (br, 2H), 4.08 (br, 2H), 1.13 (s, 6H), 3.53 (m, 2H), 1.10 (t, $J = 7.1$ Hz, 3H).

5-Ethyl-7,7-dimethyl-2-(5-methyl-1H-pyrazol-3-yl)-6-oxo-1H-imidazo[4,5-*f*]indole (2). 5-Methyl-1H-pyrazole-3-carboxylic acid (0.23 g, 1.82 mmol) and **9** (0.4 g, 1.82 mmol) were heated to 160 °C in a mixture of polyphosphoric acid (6 g) and P₂O₅ (1.68 g, 11.8 mmol) for 6 h. The mixture was poured into water (50 mL), and stirring continued until a precipitate formed. After filtration the crude product was suspended in water and neutralized by the addition of aqueous ammonia (25%). The precipitate was collected, washed with water, and dried in vacuo. Purification was achieved by chromatography on silica gel (dichloromethane/methanol 95:5), yielding 115 mg (20%) of **2** as slightly yellow solid. MS (ESI+) $m/z = 310.1$ ($M + 1$); $^1\text{H NMR}$ (400 MHz, DMSO- d_6) δ 12.90 (br, 1H), 12.60 (br, 1H), 7.39 and 7.55 (s, 1H, two tautomeric forms), 6.95 and 7.22 (s, 1H, two tautomeric forms), 6.58 (s, 1H), 3.75 (q, $J = 7.1$ Hz, 2H), 2.31 (s, 3H), 1.31 (s, 6H), 1.17 (t, $J = 7.1$ Hz, 3H). Anal. Calcd for C₁₇H₁₉N₅O: C, 66.0; H, 6.19; N, 22.64. Found C, 64.58; H, 6.09; N, 21.95.

Synthesis of Cycloalkylindolones (16–18). β -Ketoaldehydes **10–12** were synthesized as described.^{35–37} Transformation through the monophenylhydrazones **13–15** to the indole derivatives **16–18** was achieved as previously reported.^{38–40}

2,4,5,10-Tetrahydropyrazolo[3,4-*a*]carbazole (19). **17** (0.650 g, 3.51 mmol) was diluted with 20 mL of toluene and 5 mL of *N,N*-dimethylformamide dimethylacetal. The solution was heated to reflux for 20 h and then was allowed to cool to room temperature and concentrated. The residue was diluted with 20 mL of ethyl ether, and the crystalline product was collected by filtration to give 264 mg of the intermediate enamine (31%). Crude enamine (400 mg) was taken up in 50 mL of ethanol and 5 mL of hydrazine hydrate. The solution was allowed to stir for 1 week at room temperature. After removal of solvent, the residue was taken up in ethyl acetate and then washed with water and brine. The organic solution was dried and concentrated, and the residue was purified by flash column chromatography (silica gel, DCM/MeOH, 97:3) to give **19** (340 mg, 98%). MS (ESI+) $m/z = 210.1$ ($M + 1$); $^1\text{H NMR}$ (400 MHz, DMSO- d_6) δ 12.45 (s, 1H), 11.41 (s, 1H), 7.54 (s, 1H), 7.42 (d, $J = 8.0$ Hz, 1H), 7.30 (d, $J = 8.0$ Hz, 1H), 7.42 (d, $J = 8.1$ Hz, 1H), 7.06–6.94 (m, 2H), 2.94–2.80 (m, 4H); HRMS $m/z = 210.1034$ ($M + H$), calcd (C₁₃H₁₁N₃ + H) = 210.1031. HPLC purity 100%.

General Procedure for Methylpyrazole Formation. The appropriate ketone (0.500 mmol) was dissolved in 2.5–10 mL of dry THF at 0 °C. Lithium bis-trimethylsilylamide (1.25 mmol, 1 M THF solution) was added dropwise, and the mixture was stirred for 15 min at 0 °C. Acetic anhydride (1.50–7.50 mmol) was slowly added. The resulting viscous mixture was stirred for 1–12 h at

room temperature. Ethyl acetate was added, and the organic solution was washed with water and brine, dried over Na₂SO₄, and evaporated. The isolated crude intermediate was taken up in 5 mL of ethanol, which was added to 5 mL of hydrazine hydrate in 20 mL of ethanol. The solution was stirred for 12 h at room temperature. After removal of solvent and an extractive workup in ethyl acetate, the concentrated product was purified by flash column chromatography (silica gel, DCM/MeOH, 97:3) to give the desired pyrazole.

2-(5-Methyl-1H-pyrazol-3-yl)-1H-indole (20). **20** was synthesized from commercially obtained 2-acetylindole in 73% yield according to general procedure. MS (ESI+) $m/z = 198.2$ ($M + 1$); $^1\text{H NMR}$ (500 MHz, DMSO- d_6) δ 11.30 (s, 1H), 7.48 (d, $J = 7.9$ Hz, 1H), 7.36 (dd, $J = 8.0$ Hz, 1H), 7.10–6.90 (m, 2H), 6.67 (s, 1H), 6.44 (s, 1H), 2.28 (s, 3H); HRMS $m/z = 198.1033$ ($M + H$), calcd (C₁₂H₁₁N₃ + H) = 198.1031. HPLC purity 100%.

2,9-Dihydro-3-methylpyrazolo[4',3':4,5]cyclopenta[1,2-*b*]indole (21). Synthesized from **16** in 53% yield according to general procedure. MS (ESI+) $m/z = 210.2$ ($M + 1$); $^1\text{H NMR}$ (500 MHz, DMSO- d_6) δ 11.52 (s, 1H), 7.53–7.45 (m, 1H), 7.39–7.32 (m, 1H), 7.06–6.99 (m, 2H), 3.37 (s, 2H), 2.29 (s, 3H); HRMS $m/z = 210.1032$ ($M + H$), calcd (C₁₃H₁₁N₃ + H) = 210.1031. HPLC purity 98.4%.

2,4,5,10-Tetrahydro-3-methylpyrazolo[3,4-*a*]carbazole (22). **22** was synthesized from **17** in 16% yield according to general procedure. MS (ESI+) $m/z = 224.2$ ($M + 1$); $^1\text{H NMR}$ (500 MHz, DMSO- d_6) δ 11.30 (s, 1H), 7.44 (d, $J = 7.8$ Hz, 1H), 7.32 (d, $J = 8.0$ Hz, 1H), 7.06–7.00 (m, 1H), 7.00–6.94 (m, 1H), 2.90 (t, $J = 7.8$ Hz, 2H), 2.72 (t, $J = 7.7$ Hz, 2H), 2.21 (s, 3H); HRMS $m/z = 224.1187$ ($M + H$), calcd (C₁₄H₁₃N₃ + H) = 224.1188. HPLC purity 96.1%.

2,5,6,11-Tetrahydro-3-methylpyrazolo[4',3':6,7]cyclohepta[1,2-*b*]indole (23). **23** was synthesized from **18** in 7% yield according to general procedure. MS (ESI+) $m/z = 238.3$ ($M + 1$); $^1\text{H NMR}$ (500 MHz, DMSO- d_6) δ 10.85 (s, 1H), 7.40 (d, $J = 7.8$ Hz, 1H), 7.31 (d, $J = 8.0$ Hz, 1H), 7.05–6.98 (m, 1H), 6.97–6.89 (m, 1H), 3.07–2.96 (m, 2H), 2.17 (s, 3H), 2.04–1.92 (m, 2H), 2.77–2.66 (m, 2H). HPLC purity 100%.

8-Ethyl-2,5,6,12-tetrahydro-3,10,10-trimethyl-9-oxopyrazolo[4'3':6,7]cyclohepta[1,2-*b*]pyrrolo[2,3-*f*]indole (32). **32** was synthesized from **34** in 62% yield according to general procedure. MS (ESI+) $m/z = 349.3$ ($M + 1$); $^1\text{H NMR}$ (400 MHz, DMSO- d_6) δ 12.37 (s, 1H), 10.87 (s, 1H), 7.22 (s, 1H), 6.97 (s, 1H), 3.74 (q, $J = 7.0$ Hz, 2H), 3.09–2.95 (m, 2H), 2.79–2.67 (m, 2H), 2.17 (s, 3H), 2.02–1.92 (m, 2H), 1.19 (t, $J = 7.1$ Hz, 4H), 1.34–1.24 (m, 6H); HRMS $m/z = 349.2039$ ($M + H$), calcd (C₂₁H₂₄N₄O + H) = 349.2047. HPLC purity 98.2%.

2,5,6,8,12-Pentahydro-3,10,10-trimethyl-9-oxopyrazolo[4'3':6,7]cyclohepta[1,2-*b*]pyrrolo[2,3-*f*]indole (33). **33** was synthesized from **35** in 24% yield according to general procedure. MS (ESI+) $m/z = 321.1$ ($M + 1$); $^1\text{H NMR}$ (400 MHz, DMSO- d_6) δ 12.35 (s, 1H), 10.80 (s, 1H), 10.10 (s, 1H), 7.15 (s, 1H), 6.70 (s, 1H), 3.00–2.87 (m, 2H), 2.75–2.62 (m, 2H), 2.15 (s, 3H), 2.00–1.87 (m, 2H), 1.35 (s, 6H). HPLC purity 100%.

2,5,6,10,12-Pentahydro-3,8,8-trimethyl-9-oxopyrazolo[4'3':6,7]cyclohepta[1,2-*b*]pyrrolo[3,2-*f*]indole (36). **36** was synthesized from **37** in 24% yield according to general procedure. MS (ESI+) $m/z = 321.3$ ($M + 1$); $^1\text{H NMR}$ (400 MHz, DMSO- d_6) δ 12.23 (s, 1H), 10.65 (s, 1H), 10.10 (s, 1H), 7.21 (s, 1H), 6.72 (s, 1H), 3.00–2.87 (m, 2H), 2.70–2.60 (m, 2H), 2.15 (s, 3H), 2.00–1.87 (m, 2H), 1.25 (s, 6H). HPLC purity 98.9%.

3-Cyclopropyl-2,4,5,10-tetrahydropyrazolo[3,4-*a*]carbazole (24). **17** (0.200 mg, 1.08 mmol) was dissolved in 10 mL of dry THF at 0 °C. Lithium bis-trimethylsilylamide (1.30 mL, 1.30 mmol, 1 M THF solution) was added dropwise to the solution, and the mixture was stirred for 15 min. Cyclopropanoyl chloride (0.119 mL, 1.30 mmol) was slowly added and the viscous mixture stirred for 2 h at room temperature. The crude mixture was diluted with ethyl acetate, and the solution was washed with water and brine. After the mixture was dried over Na₂SO₄, solvent was removed. The residue was taken up directly in 2

mL of ethanol, which was added to 3 mL of hydrazine hydrate in 10 mL of ethanol. The solution was stirred for 12 h at room temperature. The reaction mixture was concentrated, and the residue was then taken up in ethyl acetate. The solution was washed with water and brine, and then it was dried and concentrated. The crude product was purified by flash column chromatography (silica gel, DCM/MeOH, 97:3) to give **24** (0.127 g, 47%). MS (ESI+) m/z = 250.2 (M + 1); $^1\text{H NMR}$ (500 MHz, DMSO- d_6) δ 11.30 (s, 1H), 7.45–7.31 (m, 2H), 7.10–6.91 (m, 2H), 2.85 (dq, J = 8.4 Hz, 4H), 1.90 (tt, J = 8.5, 5.2 Hz, 1H), 1.09–0.76 (m, 4H); HRMS m/z = 250.1349 (M + H), calcd (C₁₆H₁₅N₃ + H) = 250.1344. HPLC purity 98.1%.

Ethyl 3-Carboxylate-2,4,5,10-tetrahydropyrazolo[3,4-*a*]carbazole (25). **17** (0.700 mg, 3.78 mmol) was dissolved in 40 mL of dry THF at 0 °C. Lithium bis-trimethylsilylamide (9.45 mL, 9.45 mmol, 1 M THF solution) was added dropwise to the solution, and the mixture was stirred for 15 min at 0 °C. Diethyl oxylate (0.615 mL, 4.54 mmol) was slowly added. Stirring of the viscous mixture was continued for 2 h at room temperature. After addition of ethyl acetate, the organic extract was washed with water and brine and then dried. Solvent was removed, and the residue was taken up in 2 mL of ethanol. This was added to 3 mL of hydrazine hydrate in 10 mL of ethanol. The solution was stirred 3 h at room temperature. The solution was concentrated, and the resulting residue was taken up in ethyl acetate and subjected to an extractive workup. The isolated crude material was purified by flash column chromatography (silica gel, DCM/EtOH, 97:3) to give **25** (0.570 g, 54%). MS (ESI+) m/z = 280.2 (M + 1); $^1\text{H NMR}$ (400 MHz, DMSO- d_6) δ 13.78 (s, 1H), 11.32 (s, 1H), 8.18 (d, J = 7.5 Hz, 1H), 8.05 (d, J = 8.6 Hz, 1H), 7.85 (d, J = 8.4 Hz, 1H), 7.81–7.71 (m, 1H), 7.42 (t, J = 6.9 Hz, 1H), 7.25 (t, J = 7.2 Hz, 1H), 4.44 (dd, J = 13.4 Hz, 3H), 3.31 (s, 3H), 1.42 (t, J = 6.9 Hz, 4H). HPLC purity 100%.

3-Hydroxymethyl-2,4,5,10-tetrahydropyrazolo[3,4-*a*]carbazole (26). **25** (0.025 mg, 0.089 mmol) was dissolved in 5 mL of dry THF at 0 °C. Lithium aluminum hydride (0.178 mL, 0.178 mmol, 1 M THF solution) was added dropwise to the solution, which was then stirred for 15 min at 0 °C. The reaction was quenched with 1 M HCl and then concentrated. The residue was purified by HPLC (Vydac C-18 column (5 cm \times 25 cm), flow rate 20 mL/min, gradient 0–100% (0.1% TFA in water/acetonitrile), UV detector 254 nm, flow rate 20 mL/min, t_R = 52 min) to give **26** (0.016 g, 75%). MS (ESI+) m/z = 240.2 (M + 1); $^1\text{H NMR}$ (500 MHz, DMSO- d_6) δ 11.33 (s, 1H), 7.45 (d, J = 7.8 Hz, 1H), 7.32 (d, J = 8.0 Hz, 1H), 7.08–6.99 (m, 1H), 7.00–6.92 (m, 1H), 4.50 (s, 2H), 2.91 (dd, J = 11.6 Hz, 2H), 2.80 (dd, J = 11.7 Hz, 2H); HRMS m/z = 240.1143 (M + H), calcd (C₁₄H₁₃N₃O + H) = 240.1137. HPLC purity 100%.

3,3-Dimethyl-5-nitro-1H-indol-2-one (28). Compound **27**⁴¹ (38.4 g, 0.238 mol) was dissolved in 300 mL of concentrated sulfuric acid using mechanical stirring and cooled in a –40 °C bath until the reaction mixture thickened and stirring became difficult. A solution of 10.1 mL of fuming nitric acid and 50 mL of concentrated sulfuric acid was added dropwise and the mixture allowed to warm to ambient temperature with stirring over 12 h. The reaction mixture was poured into ice–water, and the precipitate was collected by filtration and dried to afford **28** (31 g, 63%). MS (ESI+) m/z = 207.2 (M + 1); $^1\text{H NMR}$ (500 MHz, DMSO- d_6) δ 11.02 (s, 1H), 8.27 (d, J = 2.4 Hz, 1H), 8.16 (dd, J = 8.6 Hz, 1H), 7.04 (d, J = 8.6 Hz, 1H), 1.33 (s, 6H).

1-Ethyl-3,3-dimethyl-5-nitro-1H-indol-2-one (30). Compound **28** (9.38 g, 40.0 mmol) was dissolved in 100 mL of DMF and added dropwise to a stirred suspension of sodium hydride (2 g, 50.0 mmol) in 25 mL of DMF. When hydrogen evolution ceased, ethyl iodide (4.00 mL, 50.0 mmol) was added. After 12 h the reaction mixture was partitioned between ethyl acetate and water. The organic extract was concentrated, and the residual solid was recrystallized from ether/hexanes to give **30** (8.52 g, 91%). $^1\text{H NMR}$ (500 MHz, DMSO- d_6) δ 8.33 (d, J = 2.4 Hz, 1H), 8.24 (dd, J = 8.7 Hz, 1H), 7.33–7.29 (m, 1H), 3.79 (q, J = 7.2 Hz,

2H), 2.51 (td, J = 3.7, 1.83 Hz, 2H), 1.4 (s, 6H), 1.17 (t, J = 7.2 Hz, 3H).

8-Ethyl-3,4,5,6-tetrahydro-10,10-dimethylcyclohepta[1,2-*b*]pyrrolo[2,3-*f*]-1H-indole, 2,9-Dione (34). **30** (8.52 g, 36.4 mmol) was suspended in 100 mL of methanol, and 1 g of 10% Pd/C catalyst was added. The resulting suspension was hydrogenated at 1 atm for 18 h. The catalyst was removed by filtration. Evaporation of the solvent gave the crude aniline **31**, which was immediately suspended in 75 mL of water. Concentrated HCl (2.3 mL) was slowly added. The resulting solution was cooled to 0 °C, and a solution of sodium nitrite (1.55 g, 22.5 mmol) in 20 mL of water was added dropwise over 10 min with vigorous stirring. This solution was added slowly to a cold (0 °C) dispersion of **12** (2.89 g, 20.6 mmol) and sodium acetate (6.9 g, 84.1 mmol) in 200 mL of water and 50 mL of methanol. After the mixture was stirred for 2 h at 0 °C, the hydrazone (4.68 g, 84%) was collected by filtration as a yellow solid. To this crude material (4.68 g, 14.3 mmol) was added 300 mL of concentrated acetic acid followed by 20 mL of concentrated HCl, and the reaction mixture was heated to 70 °C for 20 min. The solution was cooled and ~80% of the solvent removed by rotary evaporation under vacuum. The mixture was partitioned between 9:1 ethyl acetate/hexanes and washed sequentially with water, saturated sodium bicarbonate, and brine before drying over Na₂SO₄. The solvent was removed, and the crude product was recrystallized from ethyl acetate to afford **34** (2.25 g, 42%). MS (ESI+) m/z = 311.3 (M + 1); $^1\text{H NMR}$ (400 MHz, DMSO- d_6) δ 9.0 (br, 1H), 7.21 (s, 1H), 6.87 (s, 1H), 3.77 (q, J = 8.0 Hz, 2H), 3.12 (t, J = 8.0 Hz, 2H), 2.85 (t, J = 8.0 Hz, 2H), 1.93 (m, 4H), 1.37 (s, 6H), 1.25 (t, J = 8.1 Hz, 3H).

3,4,5,6-Tetrahydro-10,10-dimethylcyclohepta[1,2-*b*]-1H-pyrrolo[2,3-*f*]-1H-indole, 2,9-Dione (35). Compound **35** was synthesized in an overall yield of 82% according to the procedure given above for **34**, beginning with nitrolactam **28** and proceeding through aniline **29**. MS (ESI+) m/z = 283.3 (M + 1); $^1\text{H NMR}$ (400 MHz, DMSO- d_6) δ 11.32 (s, 1H), 10.3 (s, 1H), 7.25 (s, 1H), 6.94 (s, 1H), 3.03 (t, J = 5.6 Hz, 2H), 2.74 (m, 2H), 2.52 (m, 2H), 1.99–1.84 (m, 4H), 1.28 (s, 6H).

3,4,5,6-Tetrahydro-8,8-dimethylcyclohepta[1,2-*b*]-1H-pyrrolo[3,2-*f*]-1H-indole, 2,9-Dione (37). Compound **37** was synthesized in an overall yield of 61% as described above for **34**, beginning with nitrolactam **3** and proceeding through aniline **38**. MS (ESI+) m/z = 283.1 (M + 1); $^1\text{H NMR}$ (400 MHz, DMSO- d_6) δ 11.15 (s, 1H), 10.18 (s, 1H), 7.51 (s, 1H), 6.72 (s, 1H), 3.00 (m, 2H), 2.68 (m, 2H), 1.62 (m, 4H), 1.20 (s, 6H).

Acknowledgment. Portions of this research were carried out at the Stanford Synchrotron Radiation Laboratory, a national user facility operated by Stanford University on behalf of the U.S. Department of Energy, Office of Basic Energy Sciences. The SSRL Structural Molecular Biology Program is supported by the Department of Energy, Office of Biological and Environmental Research, and by the National Institutes of Health, National Center for Research Resources, Biomedical Technology Program, and the National Institute of General Medical Sciences. We thank members of the DMPK and Purification groups within Genentech Small Molecule Drug Discovery for analytical support and thank also the Genentech Oligonucleotide and DNA Sequencing groups.

Supporting Information Available: X-ray data collection and refinement statistics, ELISA activity comparison for wild-type and surrogate Aurora kinases, additional kinase selectivity data for inhibitor **32**, HPLC analytical data for compounds **19–26**, **32**, **33**, and **36**, and $^1\text{H NMR}$ spectra with assignments for compounds **23**, **25**, **33**, and **36**. This material is available free of charge via the Internet at <http://pubs.acs.org>.

References

- (1) Keen, N.; Taylor, S. Aurora-kinase inhibitors as anticancer agents. *Nat. Rev. Cancer* **2004**, *4*, 927–936.
- (2) Andrews, P. D. Aurora kinases: shining lights on the therapeutic horizon? *Oncogene* **2005**, *24*, 5005–5015.
- (3) Jackson, J. R.; Patrick, D. R.; Dar, M. M.; Huang, P. S. Targeted anti-mitotic therapies: can we improve on tubulin agents? *Nat. Rev. Cancer* **2007**, *7*, 107–117.
- (4) Giet, R.; Petretti, C.; Prigent, C. Aurora kinases, aneuploidy and cancer, a coincidence or a real link? *Trends Cell Biol.* **2005**, *15*, 241–250.
- (5) Carmena, M.; Earnshaw, W. C. The cellular geography of Aurora kinases. *Nat. Rev. Mol. Cell Biol.* **2003**, *4*, 842–854.
- (6) Marumoto, T.; Zhang, D.; Saya, H. Aurora A, a guardian of poles. *Nat. Rev. Cancer* **2005**, *5*, 42–50.
- (7) Meraldi, P.; Honda, R.; Nigg, E. A. Aurora kinases link chromosome segregation and cell division to cancer susceptibility. *Curr. Opin. Genet. Dev.* **2004**, *14*, 29–36.
- (8) Blangy, A.; Lane, H. A.; d'Hérin, P.; Harper, M.; Kress, M.; Nigg, E. A. Phosphorylation by p34^{cdc2} regulates spindle association of human Eg5, a kinesin-related motor essential for bipolar spindle formation in vivo. *Cell* **1995**, *83*, 1159–1169.
- (9) Giet, R.; Uzbekov, R.; Cubizolles, F.; Le Guellec, K.; Prigent, C. The *Xenopus laevis* Aurora-related protein kinase pEg2 associates with and phosphorylates the kinesin-related protein XIEg5. *J. Biol. Chem.* **1999**, *274*, 15005–15013.
- (10) Glover, D. M.; Leibowitz, M. H.; McLean, D. A.; Parry, H. Mutations in aurora prevent centrosome separation leading to the formation of monopolar spindles. *Cell* **1995**, *81*, 95–105.
- (11) Mayer, T. U.; Kapoor, T. M.; Haggerty, S. J.; King, R. W.; Schreiber, S. L.; Mitchison, T. J. Small molecule inhibitor of mitotic spindle bipolarity identified in a phenotype-based screen. *Science* **1999**, *286*, 971–974.
- (12) Hsu, J.-Y.; Sun, Z.-W.; Li, X.; Reuben, M.; Tatchell, K.; Bishop, D. K.; Gruschcow, J. M.; Brame, C. J.; Caldwell, J. A.; Hunt, D. F.; Lin, R.; Smith, M. M.; Allis, C. D. Mitotic phosphorylation of histone H3 is governed by Ipl1/aurora kinase and Glc7/PP1 phosphatase in budding yeast and nematodes. *Cell* **2000**, *102*, 279–291.
- (13) Musacchio, A.; Salmon, E. D. The spindle assembly checkpoint in space and time. *Nat. Rev. Mol. Cell Biol.* **2007**, *8*, 379–393.
- (14) Biggins, S.; Murray, A. W. The budding yeast protein kinase Ipl1/Aurora allows the absence of tension to activate the spindle checkpoint. *Genes Dev.* **2001**, *15*, 3118–3129.
- (15) Ditchfield, C.; Johnson, V. L.; Tighe, A.; Ellston, R.; Haworth, C.; Johnson, T.; Mortlock, A.; Keen, N.; Taylor, S. S. Aurora B couples chromosome alignment with anaphase by targeting BubR1, Mad2, and Cenp-E to kinetochores. *J. Cell Biol.* **2003**, *161*, 267–280.
- (16) Hauf, S.; Cole, R. W.; LaTerra, S.; Zimmer, C.; Schnapp, G.; Walter, R.; Heckel, A.; van Meel, J.; Rieder, C.; Peters, J. M. The small molecule Hesperadin reveals a role for Aurora B in correcting kinetochore-microtubule attachment and in maintaining the spindle assembly checkpoint. *J. Cell Biol.* **2003**, *161*, 281–294.
- (17) Schumacher, J. M.; Golden, A.; Donovan, P. J. AIR-2: an Aurora/Ipl1-related protein kinase associated with chromosomes and midbody microtubules is required for polar body extrusion and cytokinesis in *Caenorhabditis elegans* embryos. *J. Cell Biol.* **1998**, *143*, 1635–1646.
- (18) Kimura, M.; Matsuda, Y.; Yoshioka, T.; Okano, Y. Cell cycle-dependent expression and centrosome localization of a third human Aurora/Ipl1-related protein kinase, AIK3. *J. Biol. Chem.* **1999**, *274*, 7334–7340.
- (19) Sasai, K.; Katayama, H.; Stenoiun, D. L.; Fujii, S.; Honda, R.; Kimura, M.; Okano, Y.; Tatsuka, M.; Suzuki, F.; Nigg, E. A.; Earnshaw, W. C.; Brinkley, W. R.; Sen, S. Aurora-C kinase is a novel kinosomal passenger protein that can complement Aurora-B kinase function in mitotic cells. *Cell Motil. Cytoskeleton* **2004**, *59*, 249–263.
- (20) Li, X.; Sakashita, G.; Matsuzaki, H.; Sugimoto, K.; Kimura, K.; Hanaoka, F.; Tanaguchi, H.; Furukawa, K.; Urano, T. Direct association with inner centromere protein (INCENP) activates the novel chromosomal passenger protein, Aurora-C. *J. Biol. Chem.* **2004**, *279*, 47201–47211.
- (21) Sen, S.; Zhou, H.; White, R. A. A putative serine/threonine kinase encoding gene BTAK on chromosome 20q13 is amplified and overexpressed in human breast cancer cell lines. *Oncogene* **1997**, *14*, 2195–2200.
- (22) Bischoff, J. R.; Anderson, L.; Zhu, Y.; Mossie, K.; Ng, L.; Souza, B.; Schryver, B.; Flanagan, P.; Clairvoyant, F.; Ginther, C.; Chan, C. S. M.; Novotny, M.; Slamon, D. J.; Plowman, G. D. A homologue of *Drosophila* aurora kinase is oncogenic and amplified in human colorectal cancers. *EMBO J.* **1998**, *17*, 3052–3065.
- (23) Zhou, H.; Kuang, J.; Zhong, L.; Kuo, W.; Gray, J. W.; Sahin, A.; Brinkley, B. R.; Sen, S. Tumor amplified kinase STK15/BTAK induces centrosome amplification, aneuploidy and transformation. *Nat. Genet.* **1998**, *20*, 189–193.
- (24) Anand, S.; Penrhyn-Lowe, S.; Venkataraman, A. R. AURORA-A amplification overrides the mitotic spindle checkpoint, inducing resistance to Taxol. *Cancer Cell* **2003**, *3*, 51–62.
- (25) Zhang, D.; Hirota, T.; Marumoto, T.; Shimizu, M.; Kunitoku, N.; Sasayama, T.; Arima, Y.; Feng, L.; Suzuki, M.; Takeya, M.; Saya, H. Cre-loxP-controlled periodic Aurora-A overexpression induces mitotic abnormalities and hyperplasia in mammary glands of mouse models. *Oncogene* **2004**, *23*, 8720–8730.
- (26) Wang, X.; Zhou, Y.-X.; Qiao, W.; Tominaga, Y.; Ouchi, M.; Ouchi, T.; Deng, C.-X. Overexpression of aurora kinase A in mouse mammary epithelium induces genetic instability preceding mammary tumor formation. *Oncogene* **2006**, *25*, 7148–7158.
- (27) Harrington, E. A.; Bebbington, D.; Moore, J.; Rasmussen, R. K.; Ajose-Adeogun, A. O.; Nakayama, T.; Graham, J. A.; Demmur, C.; Hercend, T.; Diu-Hercend, A.; Su, M.; Golec, J. M. C.; Miller, K. M. VX-680, a potent and selective small-molecule inhibitor of the Aurora kinases, suppresses tumor growth in vivo. *Nat. Med.* **2004**, *10*, 262–267.
- (28) Soncini, C.; Carpinelli, P.; Gianellini, L.; Fancelli, D.; Vianello, P.; Rusconi, L.; Storici, P.; Zugnoni, P.; Pesenti, E.; Croci, V.; Ceruti, R.; Giorgini, M. L.; Cappella, P.; Ballinari, D.; Sola, F.; Varasi, M.; Bravo, R.; Moll, J. PHA-690632, a novel Aurora kinase inhibitor with potent antitumoral activity. *Clin. Cancer Res.* **2006**, *12*, 4080–4089.
- (29) Fancelli, D.; Moll, J.; Varasi, M.; Bravo, R.; Artico, R.; Berta, D.; Bindi, S.; Cameron, A.; Candiani, I.; Cappella, P.; Carpinelli, P.; Croci, V.; Forte, B.; Giorgini, M. L.; Klapwijk, J.; Marsiglio, A.; Pesenti, E.; Rocchetti, M.; Roletto, F.; Severino, D.; Soncini, C.; Storici, P.; Tonari, R.; Zugnoni, P.; Vianello, P. 1,4,5,6-Tetrahydropyrrolo[3,4-c]pyrazoles: identification of a potent Aurora kinase inhibitor with a favorable antitumor kinase inhibition profile. *J. Med. Chem.* **2006**, *49*, 7247–7251.
- (30) Manfredi, M. G.; Escedy, J. A.; Meetze, K. A.; Balani, S. K.; Burenkova, O.; Chen, W.; Galvin, K. M.; Hoar, K. M.; Huck, J. J.; LeRoy, P. J.; Ray, E. T.; Sells, T. B.; Stringer, B.; Stroud, S. G.; Vos, T. J.; Weatherhead, G. S.; Wysong, D. R.; Zhang, M.; Bolen, J. B.; Claiborne, C. F. Antitumor activity of MLN8054, an orally active small-molecule inhibitor of Aurora A kinase. *Proc. Natl. Acad. Sci. U.S.A.* **2007**, *104*, 4106–4111.
- (31) Yang, J.; Izekoe, T.; Nishioka, C.; Tasaka, T.; Taniguchi, A.; Kuwayama, Y.; Komatsu, N.; Bandobashi, K.; Togitani, K.; Koeffler, H. P.; Taguchi, H.; Yokoyama, A. AZD1152, a novel and selective Aurora B inhibitor, induces growth arrest, apoptosis, and sensitization for tubulin depolymerizing agent or topoisomerase II inhibitor in human acute leukemia cells in vitro and in vivo. *Blood* **2007**, *110*, 2034–2040.
- (32) Mortlock, A.; Keen, N. J.; Jung, F. H.; Heron, N. M.; Foote, K. M.; Wilkinson, R.; Green, S. Progress in the development of selective inhibitors of Aurora kinases. *Curr. Top. Med. Chem.* **2005**, *5*, 199–213.
- (33) Hölck, J. P.; Kampe, W.; Mertens, A.; Müller-Beckmann, B.; Strein, K.; Sponer, G. Neue Pyrrolo-Benzimidazole, Verfahren zu ihrer Herstellung und diese Verbindungen enthaltende Arzneimittel sowie Zwischenprodukte. Ger. Offen. DE 3417643, 1985.
- (34) Mertens, A.; Hölck, J. P.; Berger, H.; Müller-Beckmann, B.; Strein, K.; Roesch, E. Neue Pyrrolo-Benzimidazole, Verfahren zu ihrer Herstellung und diese Verbindungen enthaltende Arzneimittel sowie Zwischenprodukte. Ger. Offen. DE 35012497, 1986.
- (35) Johnson, W. S.; Shelberg, W. E. A plan for distinguishing between some five- and six-membered ketones. *J. Am. Chem. Soc.* **1945**, *67*, 1745–1754.
- (36) Kuhakarn, C.; Kittigowittana, K.; Pohmakotr, M.; Reutrakul, V. IBX/*n*-Bu₄NBr/CH₂Cl₂-H₂O: a new mild system for selective oxidation of secondary alcohols. *Tetrahedron* **2005**, *61*, 8995–9000.
- (37) Brückner, S.; Abraham, E.; Klotz, P.; Suffert, J. Cascade cyclization: an easy access to highly unsaturated polycyclic ring systems through a tandem Stille/[4+2] reaction under mild conditions. *Org. Lett.* **2002**, *4*, 3391–3393.
- (38) Manske, R. H. F. Synthesis of some indole derivatives. *Can. J. Res.* **1931**, *4*, 591–595.
- (39) Coffey, S. Some derivatives of 1,2-cyclohexanedione. *Recl. Trav. Chim. Pays-Bas* **1923**, *42*, 528–532.
- (40) Kavitha, C.; Prasad, K. J. R. Tetracyclic compounds from indolo[2,3-*b*]cycloheptan-1-ones. *Heterocycl. Commun.* **1999**, *5*, 481–488.
- (41) Robertson, D. W.; Krushinski, J. H.; Beedle, E. E.; Wyss, V.; Pollock, G. D.; Wilson, H.; Kauffman, R. F.; Hayes, J. S. Dihydropyridazinone cardiotonics: the discovery and inotropic activity of 1,3-dihydro-3,3-dimethyl-5-(1,4,5,6-tetrahydro-6-oxo-3-pyridazinyl)-2H-indol-2-one. *J. Med. Chem.* **1986**, *29*, 1832–1840.
- (42) Young, M. A.; Shah, N. P.; Chao, L. H.; Seeliger, M.; Milanov, Z. V.; Biggs, W. H., III; Treiber, D. K.; Patel, H. K.; Zarrinkar, P. P.; Lockhart, D. J.; Sawyers, C. L.; Kuriyan, J. Structure of the kinase domain of an imatinib-resistant Abl mutant in complex with the Aurora kinase inhibitor VX-680. *Cancer Res.* **2006**, *66*, 1007–1014.

- (43) Tyler, R. K.; Shpiro, N.; Marquez, R.; Eyers, P. A VX-680 inhibits Aurora A and Aurora B kinase activity in human cells. *Cell Cycle* **2007**, *6*, 2846–2854.
- (44) Bayliss, R.; Sardon, T.; Vernos, I.; Conti, E. Structural basis of Aurora-A activation by TPX2 at the mitotic spindle. *Mol. Cell* **2003**, *12*, 851–862.
- (45) Otwinowski, Z.; Minor, W. Processing of X-ray diffraction data collected in oscillation mode. *Methods Enzymol.* **1997**, *276*, 307–326.
- (46) Navaza, J. AMoRe: an automated package for molecular replacement. *Acta Crystallogr. A* **1994**, *50*, 157–163.
- (47) Jones, T. A.; Zou, J. Y.; Cowan, S. W.; Kjeldgaard, M. Improved methods for building protein models in electron density maps and the location of errors in these models. *Acta Crystallogr. A* **1991**, *47* (Part 2), 110–119.
- (48) Murshudov, G. N.; Vagin, A. A.; Dodson, E. J. Refinement of macromolecular structures by the maximum-likelihood method. *Acta Crystallogr. D* **1997**, *53*, 240–255.

JM800052B